Journal of Nuclear Medicine, published on June 8, 2020 as doi:10.2967/jnumed.119.240598

Monitoring response to transarterial chemoembolization in hepatocellular carcinoma using 18F-Fluorothymidine Positron Emission Tomography

Rohini Sharma[1], Marianna Inglese[1], Suraiya Dubash[1], Haonan Lu[1], David J Pinato[1], Chandan Sanghera[1], Neva Patel[1,2], Anthony Chung[1], Paul D Tait[3], Francesco Mauri[1], William R Crum[1,4], Tara D Barwick[1,3], Eric O Aboagye[1]

1. Department of Surgery and Cancer, Imperial College London, Hammersmith Hospital, Du Cane Road, W120HS London (UK).
2. Radiological Sciences Unit, Imperial College Healthcare NHS Trust
3. Department of Radiology, Imperial College Healthcare NHS Trust, London
4. Institute of Translational Medicine and Therapeutics, Imperial College London

Running Head: Imaging proliferation in liver cancer

Word Count: 4998 **Tables:** 2 **Figures:** 2 **Supplemental Figures:** 3

Keywords: 18F-FLT-PET, hepatocellular cancer, response,

***To whom correspondence should be addressed:**

Dr Rohini Sharma MBBS, FRACP, PhD, FRCP

Reader in Oncology and Clinical Pharmacology

Imperial College London, Hammersmith Campus, Du Cane Road,

W12 0HS, London (UK)

Tel: +4420 83833720

E mail: r.sharma@imperial.ac.uk

ABSTRACT

Accurate disease monitoring is essential following transarterial chemoembolization (TACE) in hepatocellular carcinoma (HCC) due to potential for profound adverse event and large variation in survival outcome. Post-treatment changes on conventional imaging can confound determination of residual/recurrent disease, magnifying the clinical challenge. Based on increased expression of thymidylate synthase (TYMS), thymidine kinase-1 (TK-1) and SLC29A1 (Equilibrative nucleoside transporter 1, ENT1) in HCC compared with liver tissue, we conducted a proof of concept study evaluating the efficacy of 18F-fluorothymidine (18F-FLT)-PET to assess response to TACE. As previous PET studies in HCC have been hampered by high background liver signal, we investigated if a temporal-intensity voxel-clustering ("Kinetic Spatial Filtering") (KSF) improved lesion detection.

Methods A tissue microarray (TMA) was built from 36 HCC samples and matched surrounding cirrhotic tissue and was stained for thymidine kinase-1 (TK-1). A prospective study was conducted; eighteen patients with a diagnosis of HCC by American Association for the Study of Liver Diseases criteria (AALSD) who were eligible to treatment with TACE were enrolled. Patients underwent baseline conventional imaging and dynamic 18F-FLT-PET/KSF followed by TACE. Repeat imaging was performed 6-8 weeks post TACE. PET parameters were compared with modified-Response Evaluation in Solid Tumours (mRECIST) enhancement-based criteria.

Results Cancer Genome Atlas analysis revealed increased RNA expression of *TYMS*, *TK-1* and *SLC29A1* in HCC. TK-1 protein expression was significantly higher in HCC ($p<0.05$). The sensitivity of 18F-FLT-PET for baseline HCC detection was 73% (SUV_{max} of 9.7 ± 3.0; tumour to liver ratio of 1.2 ± 0.3). Application of KSF did not improve lesion detection. Lesion response following TACE by mRECIST criteria was 58% (14 patients with 24 lesions). A 30% reduction in mean 18F-FLT-PET uptake was observed following TACE correlating to an observed PET response of 60% (n=15/25). A significant and profound reduction in radiotracer delivery parameter, K1, following TACE was observed.

Conclusion 18F-FLT-PET can differentiate HCC from surrounding cirrhotic tissue, with PET parameters correlating with TACE response. KSF did not improve visualization of tumour lesions. These findings warrant further investigation.

INTRODUCTION

The recommended treatment option for intermediate stage hepatocellular cancer (HCC) is transarterial chemoembolisation (TACE), which involves the delivery of a cytotoxic agent commonly mixed with lipiodol followed by selective embolization of the tumoural arterial supply(*1*). The typical vascular pattern of HCC on contrast enhanced-CT or MRI is early arterial enhancement followed by "washout". Whilst both contrast-enhanced CT and MRI are widely used to assess response post TACE, there is uncertainty in their ability to detect viable disease post TACE(*2*). Modified RECIST criteria, which measure changes in arterial enhancement as a marker of residual viable tumour, is a more accurate measure of tumour response to treatment than standard RECIST and is routinely used in the assessment of HCC(*3*). However, lipiodol deposition can induce beam-hardening artefact and obscure enhancement on arterial phase, reducing the sensitivity of CT post TACE. With MRI, coagulative haemorrhagic necrosis may lead to high T1 signal making enhancement assessment difficult(*4*).

PET imaging has been evaluated in HCC for staging and response assessment(*5*). Studies investigating 18F-fluorodeoxyglucose (18F-FDG) in HCC show limited sensitivity (50 –70%) due to similar activities of glycolytic enzymes and glucose 6-phosphatase in liver and well-differentiated HCC resulting in near equivalent uptake of 18F-FDG(*6*). Imaging with single agent 11C-acetate and 11C-, 18F-choline are similarly limited, culminating in the exploitation of dual-tracer techniques to improve sensitivity and specificity(*7*).

3'-Deoxy-3'-18F-fluorothymidine (18F-FLT) is a surrogate marker of proliferation, with uptake reflecting the activity of thymidine kinase (TK-1) whose expression correlates with *ex vivo* proliferation biomarkers(*8*). Unlike 18F-FDG, the uptake of 18F-FLT is more specific for proliferation and is unaffected by inflammation, a particular concern as HCC tumours develop within a pro-inflammatory milieu(*9*). To date a single study of 18F-FLT-PET in HCC indicated that 69% of patients had uptake higher than background liver, whilst the remaining lesions were either photopaenic or of mixed uptake(*10*). However, the patient group was heterogeneous including cholangiocarcinoma, and no information was given regarding therapy response. To improve lesion detection, we have previously applied a temporal voxel-clustering approach—Kinetic Spatial Filter (KSF)—for removing normal, physiological hepatic 18F-FLT uptake and to visualise specific uptake (i.e. uptake due to phosphorylation) in liver

metastases(*11*). Briefly, the KSF compares the time-activity curves (TACs) of each voxel with the TAC of predefined tissue classes such as liver and tumour. Voxels classed as “liver-like” are excluded, thereby removing areas of physiological uptake unrelated to 18F-FLT retention.

This study evaluates the clinical utility of 18F-FLT-PET in assessing TACE response in HCC. We first reviewed RNA expression of key targets in the metabolism of FLT using large published datasets of HCC. We then investigated the tissue expression of TK-1 in HCC and surrounding cirrhosis, an important consideration in developing a tracer paradigm that will effectively differentiate cirrhotic tissue and HCC. Finally we undertook a prospective study using dynamic 18F-FLT-PET to both visualise the tumours and use as a response biomarker, incorporating application of the KSF and kinetic modelling.

MATERIALS AND METHODS

Bioinformatics Analysis

RNA-sequencing dataset containing 371 HCC and 50 non-malignant tissue from The Cancer Genome Atlas (TCGA) project was measured from Illumina HiSeq 2000 RNA Sequencing platform. The RSEM normalized data was downloaded from UCSC Xena (http://xena.ucsc.edu/). Differential gene expression of *TK1*, *TYMS* and *SLC29A1* comparing tumour and non-malignant tissue were performed using 'ggplot2' package and 't.test' function in R 3.5.2.

Tissue Microarray

Immunohistochemistry for TK-1 (1:100, AbCam, Cambridge) was performed on a tissue microarray (TMA) from patients with a histological diagnosis of HCC (n=36)(Supplemental Methods and Materials). A trained histopathologist (FM) blinded to the clinical data scored all cases manually using the immunohistochemical score(*12*).

Prospective Study Design

Eighteen patients with HCC were prospectively enrolled. Patients received standard TACE with liposomal doxorubicin emulsified in lipiodol followed by embolisation with gelatin sponge particles. Baseline staging included contrast CT and/or MRI liver conducted 28 days prior to TACE and the same imaging modality repeated 6-8 weeks following TACE for treatment response, and then 3-monthly until disease progression. Modified RECIST (mRECIST) for HCC(*13*) was documented by a single experienced hepatobiliary radiologist (PT) (Supplemental Methods and Materials). .

Image Analysis

Lesions on 18F-FLT-PET corresponding to those on the CT or MRI greater than 10mm, and showing an increased uptake were considered as target lesions and used for analyses on both the PET/CT and CT or MRI, before and after treatment.

Consecutive regions of interest (ROI) were manually defined on the summed images and encompassed the whole tumour for SUV analysis. 18F-FLT radioactivity concentration within the ROIs was normalised for injected radioactivity and body weight (grams) to obtain mean and maximum SUV at 60 minutes ($SUV60_{mean}$, and $SUV60_{max}$) on baseline and post-treatment 18F-FLT PET/CT studies. The percentage change in SUV in both SUV_{mean} and SUV_{max} was calculated for each target lesion visible on baseline imaging as; $(SUV_{post} - SUV_{pre})/SUV_{pre}$. In each case, a 3cm ROI was placed in the liver in a tumour-free area to measure background liver SUV_{mean} , and the tumour/liver (T/L) ratio (Tumour SUV_{max} /Liver SUV_{mean}) determined.

Quantitative Analysis

A metabolite-corrected image-derived arterial input function was implemented during kinetic modelling of data with a two-tissue compartmental model (Supplemental Material and Methods – Quantitative Analysis).

Statistical Analysis

As this was a pilot study, no formal power calculation was undertaken. Summary statistics of the associations between PET parameters and clinical outcome were determined. Due to the small sample size, patients were grouped as responders (complete and partial response, CR and PR) or non-responders (stable disease or progressive disease, SD and PD). The relationship between kinetic parameters and response was evaluated using Wilcoxon rank tests. Chi-squared test was used to evaluate utility of the tracer pre- and post-TACE therapy. Concordance was determined using Cohen's kappa analysis. $P \leq 0.05$ was considered significant. All statistical analyses were conducted using SPSS statistical package version 22 (SPSS Inc., Chicago, IL, USA).

RESULTS

Expression of Enzymes Involved in Thymidine Metabolism increased in HCC Compared with Cirrhotic tissue

Using RNA-sequencing data from The Cancer Genome Atlas we observed a significantly higher expression of *TYMS*, *TK-1* and *SLC29A1* in tumour tissue (n=371) compared to adjacent non-malignant tissue (n=50; $p<0.05$) (Supplemental Figs. 1A, B and C). Using a TMA we observed a significantly higher TK-1 expression in HCC (median immunohistochemical score 33, range 0 - 300) compared to the surrounding parenchyma (score 0, range 0 – 50), suggesting that 18F-FLT has the potential to differentiate HCC from surrounding cirrhotic liver ($p=0.004$) (Supplemental Figs. 2 A, B and C).

Patient Characteristics

Eighteen patients were enrolled (16 men and 2 women) with 16 patients completing the study. (Table 1). Median age was 68 years (range 42–79years). All patients received TACE for intermediate stage disease. Three patients had had previous TACE and were undergoing retreatment for residual active disease; the remaining patients were treatment naïve.

HCC is Visible Above Background Liver Using 18F-FLT-PET Imaging

Twenty-six liver lesions, median 29.5mm (range 10-117mm) were identified on conventional imaging; five had baseline MRI and the remainder CT. On PET visual analysis, 19 lesions were visible above background liver (73% sensitivity)(Figs. 1A-F).

All lesions were included in analysis. The mean $SUV_{60,mean}$ (±SD) and $SUV_{60,max}$ on baseline imaging were 6.5 (±1.9) and 9.7 (±3.0), respectively. The mean $SUV_{60,mean}$ of the background liver was 6.1 (±0.9). A significant difference was observed between $SUV_{60,max}$ of the cancer compared to surrounding, non-cancerous liver tissue ($p=0.02$), with the mean tumour to liver (T/L) ratio being 1.2 (±0.3), confirming that uptake in HCC was above cirrhotic background activity, enabling visualization on 18F-FLT-PET scans in most cases.

Application of Kinetic Filter Does Not Improve Visualization of HCC on Cirrhotic Liver Background

Background liver activity was completely filtered out in 12/16 patients; 4/16 patients retained partial background liver activity. KSF did not improve image visualisation above that of PET/CT imaging; 11 of the 26 lesions (42%) were visible following application of KSF compared with 19 lesions without KSF (Figs.2A-F). Small lesions typically had a homogeneous appearance, whereas larger lesions were characterised by perilesional tracer uptake with no measurable FLT trapping in the necrotic centre of tumour. Of the 15 lesions not visualised by the KSF, 9 (60%) were <30 mm; 3 lesions had higher tissue activity than the average for HCC predetermined by the KSF and the remaining lesions did not retain radiotracer following application of the filter. As KSF is associated with removal of delivery components within the data, there was a mean (range) signal reduction in the tumours at baseline of 81% (18–100%) relative to the unfiltered images. The mean reduction in background activity in the liver was 98% (83-100%), resulting in an improved T/L ratio of 11.1 ± 17.7.

18F-FLT Uptake Parameters and Clinical 0utcome

In terms of response to TACE according to mRECIST criteria, 24 lesions were assessable; two lesions were not assessable (one patient withdrew consent following baseline PET). Response was observed in 14/24 (58%) and non-response in 10/24 (42%) lesions. There was a median overall reduction in 18F-FLT-PET/CT $SUV_{60,\,mean}$ (-29.5% ± 31.4%) and $SUV_{60,\,max}$ (-18.5% ± 27.5 %) following TACE. Previous test–retest reproducibility studies in breast cancer considered changes in 18F-FLT SUV of more than 20% as significant (SD: 10%–15%)(*14*). Using a 20% reduction in $SUV_{60,\,mean}$ to define PET response led to categorization of lesional response in 60% (N=15/25) and non-response in 40% (n=10/25). Using Cohen's kappa measures, there was good concordance between lesional PET response and lesional mRECIST (κ 0.66, p<0.001, 95% CI 0.35 – 0.97).

Kinetic Modelling Illustrates Significant Reduction in 18F-FLT Uptake and Retention Following TACE

The analysis of 18F-FLT dynamic data with a two tissue compartmental model resulted in physiologically relevant kinetic parameters(N=14) (Table 2)(*15*). There was a significant reduction in mean K_1 values from baseline, 0.3±0.1 (mL/min/g), compared to post-treatment, 0.13 ± 0.05 (p<0.001). This is consistent with the abrupt cessation of blood flow to the tumour following embolization resulting in reduced transport of 18F-FLT to the tumour. While all tumours showed some degree of reduction in K_1, the change was greater in responders (66%

reduction) versus non-responders (50%), p=0.03 (Supplemental Fig. 3A). Baseline $SUV_{60, mean}$ and baseline K_i were significantly correlated (Pearson's correlation coefficient 0.5, p=0.04) and a significant difference was observed in K_i at baseline 0.09 $\pm$ 0.03 (mL/min/g) compared to post-TACE imaging, 0.04 $\pm$ 0.02 ($p<0.001$). In responders, baseline K_i and v_B were greater compared to non-responders (Supplemental Figs. 3B and C)($p<0.05$).

DISCUSSION

There is still no single tracer recommended by international guidelines for either diagnosis or response assessment in HCC(*1*). The main limitation of the studied tracers has been poor tumour- to-background liver ratio resulting in a dual tracer approach for visualizing HCC, which is time-consuming and exposes patients to significant radiation(*5*). We hypothesized, that as 18F-FLT uptake is specific for tumour proliferation, tracer uptake will not be affected by the presence of inflammation(*16*). Moreover, we investigated the utility of KSF to improve visualization of HCC by removing background liver activity.

In order to address the hypothesis that tumour 18F-FLT uptake will change predictably with effective treatment, we first assessed the mRNA expression of factors responsible for handling 18F-FLT. TYMS catalyses the last step in the de novo synthesis of thymidine monophosphate (TMP) whilst TK-1 catalyses synthesis of TMP via the salvage pathway. TK-1 impacts on 18F-FLT cellular trapping and is a surrogate marker of proliferation(*17*). Moreover, we have shown that with TYMS inhibition, 18F-FLT uptake increases due to redistribution of the membrane transporter SLC29A1 to the plasma membrane(*18*). Expression levels of *TYMS, TK-1* and *SLC29A1* were all markedly upregulated in HCC compared to normal liver; we confirmed marked upregulation in protein expression of TK-1 in HCC compared to surrounding matched cirrhotic tissue consisting of both regenerative and dysplastic nodules suggesting that 18F-FLT could be useful in differentiating HCC from surrounding cirrhotic tissue.

Our prospective 18F-FLT-PET study illustrated that the majority of intrahepatic lesions, had increased tracer uptake above background liver consistent with the TMA findings. To improve HCC visualization, we applied the previously validated KSF(*19,20*). However, fewer lesions were detected with the filter than with standard PET/CT imaging; the majority of small lesions, <3cm, were filtered out. Possible explanations are: (i) the KSF compares voxel temporal profiles with standard tissue profiles and both liver and lesion voxel profiles were highly variable in our group; (ii) the cirrhotic background has a high relative uptake which, in combination with (i), reduces the ability of the KSF to effectively discriminate HCC from the proliferating, background liver, (iii) partial volume effects may contribute to filtering out of small lesions.

When considering 18F-FLT-PET imaging for lesion detection, our findings are in keeping with Eckels and colleagues who reported a 72% sensitivity of 18F-FLT in visualizing HCC with similar median SUV and T/L ratios(*10*). Similar sensitivities have been reported with 11C-acetate-PET and with a dual tracer approach with 18F-FDG and 11C-acetate, 75% and 73%, respectively(*21,22*). However, Ho and colleagues report single tracer sensitivity of 87% with 11C-acetate, increasing to 100% sensitivity using two tracers(*23*). These differences in diagnostic sensitivity maybe a reflection of the subgroup analysis undertaken in the Ho paper. Overall, the literature does suggest improved diagnostic sensitivity using a dual tracer approach, which motivates the development of alternate tracers for the detection of HCC.

We investigated the role of dynamic 18F-FLT-PET as a predictor of TACE response. The radiologic response to TACE by mRECIST was 54%, and by PET was 60%, with good concordance between imaging modalities observed. Cascales-Campos and colleagues considered using 18F-FDG-PET to assess response to TACE prior to liver transplantation(*24*). The authors describe a reduction in 18F-FDG uptake correlating with degree of necrosis on pathologic examination of the explanted liver, and other investigators have considered minimum SUV cut-off values for defining response to therapy(*25*). In a retrospective study, Park and colleagues investigated the utility of a dual tracer approach with 18F-FDG and 11C-acetate in predicting response to TACE. They did not investigate concordance between the imaging modalities but observed that the ratio of 18F-FDG to 11C-acetate predicted response to TACE determining a cut off from ROC analysis(*7*). We selected a 20% reduction in $SUV_{60,\ max}$ to indicate response, a cut-off extrapolated from breast cancer studies(*26*). Larger studies are needed to define a more accurate cut-off for HCC than was possible to derive from our small data-set.

A key strength of this study is that dynamic PET imaging allows us to establish the basis of the PET signal change in HCC, considering that TACE acutely impacts on blood flow. In line with our hypothesis, we report a significant reduction in K_1 following TACE, illustrating abrupt reduction in tissue perfusion. This is in sharp contrast with anti-angiogenic chemotherapy where an increase in the K_1 due to vessel normalization and reduced interstitial pressure can accompany response(*27*). Dynamic studies using 11C-acetate report a reduced K_1 in HCC lesions supplied by the hepatic artery compared with benign lesions supplied by the portal vein as the radiotracer concentration time-course is initially delayed in the portal vein as passes through the splanchnic circulation(*28*).

Huo and colleagues reported that because of the differential time-course of radiotracers circulating through the hepatic artery or portal vein, lesions supplied by the hepatic artery will reach “stable concentration” of radiotracer earlier and at a higher peak following injection; hence arterialized lesions will have a lower K_1 compared to benign lesions that are supplied predominantly by the portal vein(*29*). K_i is the metabolic flux constant and it is related to the phosphorylation of the thymidine in the tissue(*30*). It has previously found to be correlated to 18F-FLT SUV(*31*); and our results illustrate similar correlation. Moreover, we report baseline K_i and v_B to be predictive of TACE response to treatment suggesting that responding tumours are more actively proliferating and have higher perfusion suggestive of higher vascularity.

Study limitations include small sample size and lack of correlation of PET uptake parameters with histology. If subjects had whole body imaging full assessment of extra-hepatic disease could be performed; correlation of PET kinetic parameters with SUV means that future whole body static imaging would be supported. In addition manual VOIs could not be used to determine thresholds as components of the tumour were close to background liver activity. In addition, some lesions became isointense/photopenic relative to background on follow- up PET imaging.

In summary, we have shown that TK-1 expression is significantly higher in HCC compared to surrounding cirrhotic tissue supporting the use of 18F-FLT-PET. High 18F-FLT-PET uptake is seen in the majority of HCC, however application of KSF did not improve visualization due to high and variable SUV both in tumour and background cirrhotic liver. Imaging proliferation with 18F-FLT-PET may be used to predict response to TACE in this small case series. Whilst this study is a pilot study, the results generated are provocative and should be taken forward to larger prospective trials correlating with outcome.

DISCLOSURES

No authors have any conflicts of interest to declare.

ACKNOWLEDGEMENTS

Kasia Kowlozski, Robert Punjani, Hope McDevitt, Vijay Vaja. This research study was supported by the Imperial College NIHR Imperial Biomedical Research Centre and Imperial College Experimental Cancer Medicines Centre. The views expressed are those of the authors and not necessarily those of the NIHR or the Department of Health and Social Care.

FINANCIAL SUPPORT

Imperial Experimental Cancer Medicines Centre, Cancer Research UK (C2536/A16584).

KEY POINT QUESTION

Does dynamic 18F-FLT-PET allow accurate visualisation of HCC?

PERTINENT FINDINGS

18F-FLT-PET can differentiate HCC from surrounding cirrhotic tissue, with PET parameters correlating with TACE response.

IMPLICATIONS FOR PATIENT CARE

18F-FLT-PET can accurately detect HCC and should be further investigated, particularly for assessment of response.

REFERENCES

1. European Association for the Study of the Liver. Electronic address eee, European Association for the Study of the L. EASL Clinical Practice Guidelines: Management of hepatocellular carcinoma. *J Hepatol.* 2018;69:182-236.

2. Chapman WC, Majella Doyle MB, Stuart JE, et al. Outcomes of neoadjuvant transarterial chemoembolization to downstage hepatocellular carcinoma before liver transplantation. *Annals of surgery.* 2008;248:617-625.

3. Gordic S, Corcuera-Solano I, Stueck A, et al. Evaluation of HCC response to locoregional therapy: Validation of MRI-based response criteria versus explant pathology. *J Hepatol.* 2017;67:1213-1221.

4. Kim S, Mannelli L, Hajdu CH, et al. Hepatocellular carcinoma: assessment of response to transarterial chemoembolization with image subtraction. *J Magn Reson Imaging.* 2010;31:348-355.

5. Bieze M, Klumpen HJ, Verheij J, et al. Diagnostic accuracy of 18F-methyl-choline PET/CT for intra- and extrahepatic hepatocellular carcinoma. *Hepatology.* 2013.

6. Weber G, Morris HP. Comparative Biochemistry of Hepatomas. Iii. Carbohydrate Enzymes in Liver Tumors of Different Growth Rates. *Cancer Res.* 1963;23:987-994.

7. Park S, Kim TS, Kang SH, Kim HB, Park JW, Kim SK. 11C-acetate and 18F-fluorodeoxyglucose positron emission tomography/computed tomography dual imaging for the prediction of response and prognosis after transarterial chemoembolization. *Medicine (Baltimore).* 2018;97:e12311.

8. Toyohara J, Waki A, Takamatsu S, Yonekura Y, Magata Y, Fujibayashi Y. Basis of FLT as a cell proliferation marker: comparative uptake studies with [3H]thymidine and [3H]arabinothymidine, and cell-analysis in 22 asynchronously growing tumor cell lines. *Nucl Med Biol.* 2002;29:281-287.

9. van Waarde A, Jager PL, Ishiwata K, Dierckx RA, Elsinga PH. Comparison of sigma-ligands and metabolic PET tracers for differentiating tumor from inflammation. *J Nucl Med.* 2006;47:150-154.

10. Eckel F, Herrmann K, Schmidt S, et al. Imaging of proliferation in hepatocellular carcinoma with the in vivo marker 18F-fluorothymidine. *Journal of nuclear medicine : official publication, Society of Nuclear Medicine.* 2009;50:1441-1447.

11. Gray KR, Contractor KB, Kenny LM, et al. Kinetic filtering of [(18)F]Fluorothymidine in positron emission tomography studies. *Phys Med Biol.* 2010;55:695-709.

12. Pinato DJ, Ramachandran R, Toussi ST, et al. Immunohistochemical markers of the

hypoxic response can identify malignancy in phaeochromocytomas and paragangliomas and optimize the detection of tumours with VHL germline mutations. *Br J Cancer.* 2013;108:429-437.

13. Lencioni R, Llovet JM. Modified RECIST (mRECIST) assessment for hepatocellular carcinoma. *Semin Liver Dis.* 2010;30:52-60.

14. Kenny L, Coombes RC, Vigushin DM, Al-Nahhas A, Shousha S, Aboagye EO. Imaging early changes in proliferation at 1 week post chemotherapy: a pilot study in breast cancer patients with 3'-deoxy-3'-[18F]fluorothymidine positron emission tomography. *Eur J Nucl Med Mol Imaging.* 2007;34:1339-1347.

15. Contractor K, Challapalli A, Tomasi G, et al. Imaging of cellular proliferation in liver metastasis by [18F] fluorothymidine positron emission tomography: effect of therapy. *Physics in Medicine & Biology.* 2012;57:3419.

16. van Waarde A, Cobben DC, Suurmeijer AJ, et al. Selectivity of 18F-FLT and 18F-FDG for differentiating tumor from inflammation in a rodent model. *Journal of nuclear medicine : official publication, Society of Nuclear Medicine.* 2004;45:695-700.

17. Kenny LM, Vigushin DM, Al-Nahhas A, et al. Quantification of cellular proliferation in tumor and normal tissues of patients with breast cancer by [18F]fluorothymidine-positron emission tomography imaging: evaluation of analytical methods. *Cancer research.* 2005;65:10104-10112.

18. Perumal M, Pillai RG, Barthel H, et al. Redistribution of nucleoside transporters to the cell membrane provides a novel approach for imaging thymidylate synthase inhibition by positron emission tomography. *Cancer Res.* 2006;66:8558-8564.

19. Challapalli A, Barwick T, Pearson RA, et al. 3'-Deoxy-3'-(1)(8)F-fluorothymidine positron emission tomography as an early predictor of disease progression in patients with advanced and metastatic pancreatic cancer. *Eur J Nucl Med Mol Imaging.* 2015;42:831-840.

20. Contractor K, Challapalli A, Tomasi G, et al. Imaging of cellular proliferation in liver metastasis by [18F]fluorothymidine positron emission tomography: effect of therapy. *Phys Med Biol.* 2012;57:3419-3433.

21. Li S, Peck-Radosavljevic M, Ubl P, et al. The value of [(11)C]-acetate PET and [(18)F]-FDG PET in hepatocellular carcinoma before and after treatment with transarterial chemoembolization and bevacizumab. *Eur J Nucl Med Mol Imaging.* 2017;44:1732-1741.

22. Park JW, Kim JH, Kim SK, et al. A prospective evaluation of 18F-FDG and 11C-acetate PET/CT for detection of primary and metastatic hepatocellular carcinoma. *J Nucl Med.* 2008;49:1912-1921.

23. Ho CL, Yu SC, Yeung DW. 11C-acetate PET imaging in hepatocellular carcinoma and

other liver masses. *J Nucl Med.* 2003;44:213-221.

24. Cascales-Campos PA, Ramirez P, Lopez V, et al. Prognostic Value of 18-Fluorodeoxyglucose-Positron Emission Tomography After Transarterial Chemoembolization in Patients With Hepatocellular Carcinoma Undergoing Orthotopic Liver Transplantation. *Transplant Proc.* 2015;47:2374-2376.

25. Lee JW, Yun M, Cho A, et al. The predictive value of metabolic tumor volume on FDG PET/CT for transarterial chemoembolization and transarterial chemotherapy infusion in hepatocellular carcinoma patients without extrahepatic metastasis. *Ann Nucl Med.* 2015;29:400-408.

26. Kenny L, Coombes RC, Vigushin DM, Al-Nahhas A, Shousha S, Aboagye EO. Imaging early changes in proliferation at 1 week post chemotherapy: a pilot study in breast cancer patients with 3'-deoxy-3'-[18F]fluorothymidine positron emission tomography. *European journal of nuclear medicine and molecular imaging.* 2007;34:1339-1347.

27. Scarpelli M, Simoncic U, Perlman S, Liu G, Jeraj R. Dynamic (18)F-FLT PET imaging of spatiotemporal changes in tumor cell proliferation and vasculature reveals the mechanistic actions of anti-angiogenic therapy. *Phys Med Biol.* 2018;63:155008.

28. Winterdahl M, Keiding S, Sorensen M, Mortensen FV, Alstrup AK, Munk OL. Tracer input for kinetic modelling of liver physiology determined without sampling portal venous blood in pigs. *Eur J Nucl Med Mol Imaging.* 2011;38:263-270.

29. Huo L, Guo J, Dang Y, et al. Kinetic analysis of dynamic (11)C-acetate PET/CT imaging as a potential method for differentiation of hepatocellular carcinoma and benign liver lesions. *Theranostics.* 2015;5:371-377.

30. Muzi M, Spence AM, O'Sullivan F, et al. Kinetic analysis of 3′-deoxy-3′-18F-fluorothymidine in patients with gliomas. *Journal of Nuclear Medicine.* 2006;47:1612-1621.

31. Muzi M, Vesselle H, Grierson JR, et al. Kinetic analysis of 3′-deoxy-3′-fluorothymidine PET studies: validation studies in patients with lung cancer. *Journal of Nuclear Medicine.* 2005;46:274-282.

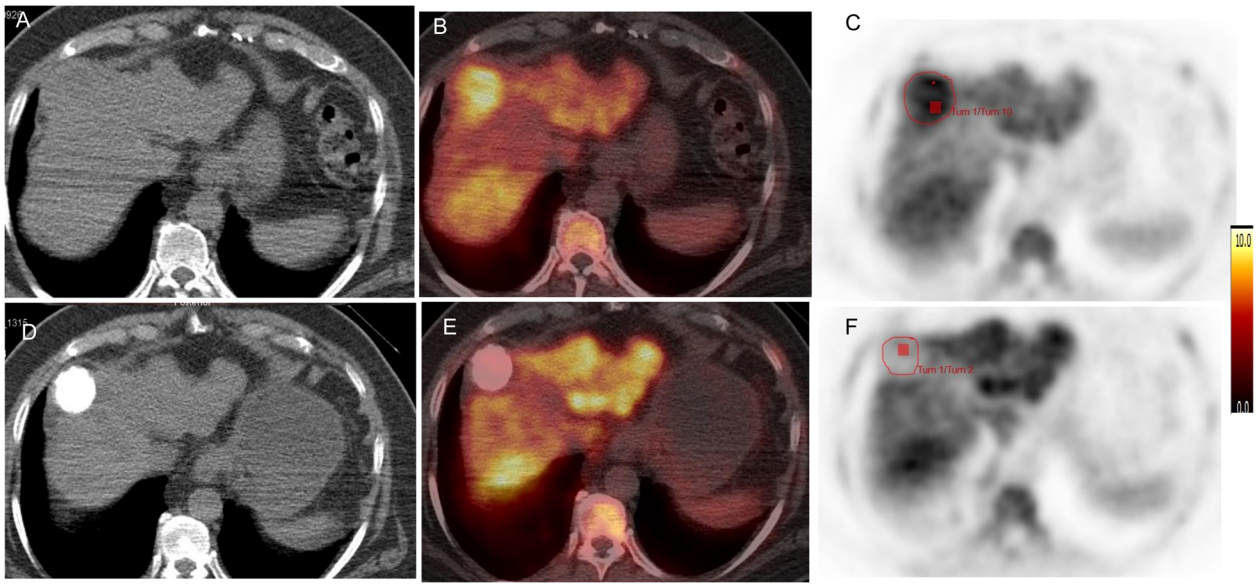

FIGURE 1. Axial CT, Fused and FLT PET images pre-(**A, B, C**) and post-(**D, E, F**) TACE show focal HCC lesion (red outline) with increased FLT uptake at baseline and reduction post TACE.

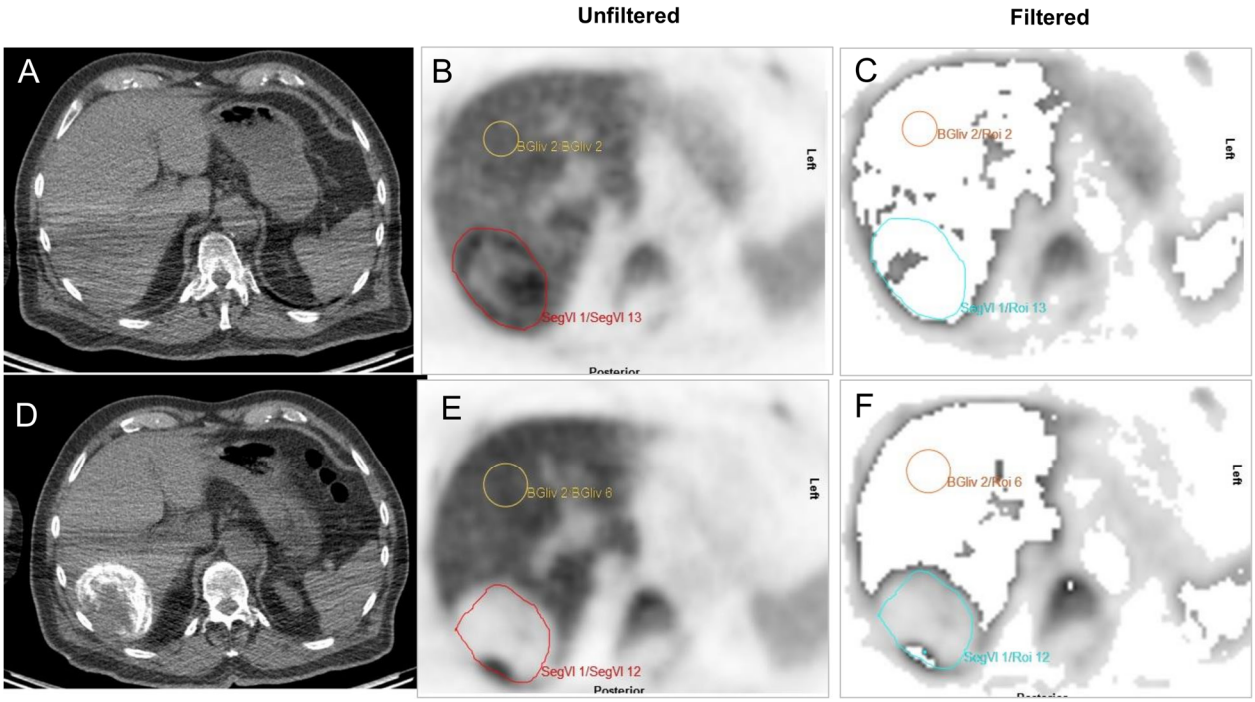

FIGURE 2. Axial CT, unfiltered PET and filtered PET images pre-(**A, B, C**) and post-(**D, E, F**) TACE show focal HCC lesion (red outline) with increased FLT uptake at baseline and reduction post TACE. Images **B** and **E** indicate PET images prior to application of KSF where at baseline **(B**) HCC is visible above background. Following application of the filter, the tumour is mostly filtered out (**C**). In the post TACE images, the HCC is photopaenic compared to surrounding liver prior to application of the filter (**E**). Following application, the background liver activity is removed and the HCC remains visible (**F**)

Table 1. Imaging features of HCC lesions

Patient	Lesion location	Size (mm)	Uptake above background liver (visual)	Background liver SUVmean	$SUV_{60,ave}$ x $10^{-5}m^2mL^{-1}$ (preRx)	$SUV_{60,max}$ x $10^{-5}m^2mL^{-1}$ (preRx)	mRECIST response	Percentage Change $SUV_{60,ave}$	Percentage Change $SUV_{60,max}$	Progression Free Survival (months)
1	Diffuse disease, R lobe	117	Isotense	4.3	3.4	5.1	PR	-12.2	13.9	3
2	Segment V/VI	56	Hyperintense rim/ hypointense centre	4.9	4.3	7.8	PR	-55.5	-45.5	6.6
3	Segment VII	60	Isotense	6.3	5.7	7.9	SD	-65.2	-42.6	5.3
4	Segment VI	20	Isotense	5.5	2.8	5.5	SD	-6.0	-14.4	4.5
4	Segment V	52	Isotense	5.5	4.1	5.8	SD	-0.9	-6.7	
5	Segment II	44	Hyperintense	6.6	7.5	10.3	SD	-37.4	1.4	11.4
	Segment VI[c]	24	Hyperintense	6.6	7.6	9.9	SD	10.9	-0.7	
	Segment IV	19	Hyperintense	6.6	7.3	9.8	SD	15.5	26.2	
	Segment IV	16	Hyperintense	6.6	7.8	10.3	SD	5.9	1.9	
	Segment VIII	15	Hyperintense	6.6	7.1	9.4	SD	0.07	0.9	
	Segment IV	13	Hyperintense	6.6	7.8	11.3	SD	-4.7	0.9	
	Segment VIII	19	Hyperintense	6.6	7.1	8.2	PR	22.2	36.5	
6	Segment III	22	Hyperintense	4.8	7.6	10.2	NE	-69.2	-61.9	17.3
7	Segment III	22	Hyperintense	6.1	10.9	14.3	NE	NE	NE	8.0
8	Segment VIII	42	Hyperintense	6.5	7.8	11.5	PR	-66.4	-41.5	1.5
9	Segment II	28	Hyperintense	6.3	7.9	10.3	CR	-58.6	-46.1	5.2
10	Segment I	62	Hyperintense	7.7	8.1	20.4	PR	-71.3	-41.0	1.1[e]
11	Segment III	38	Hyperintense	6.1	7.1	10.6	PR	-29.0	-21.5	7.8
12	Segment VIII	59	Mixed isotense/hypotense	8.0	5.1	10.9	PR	-55.8	-32.8	16.7
12	Segment IV[d]	60	Hypotense	8.0	2.9	8.4	PR	-51.6	-33.9	
13	Segment VI	31	Hyperintense	4.8	6.4	8.9	CR	-39.4	-48.6	19.1
14	Segment VII (sagittal)	18	Hyperintense	5.3	5.3	7.4	CR	-33.9	-30.5	8.1
14	Segment VIII	26	Hyperintense	5.3	6.3	7.5	CR	-33.5	-39.1	
14	Segment VII (medial)	10	Hyperintense	5.3	6.6	8.0	SD	17.2	30.9	
15	Segment VIII	34	Hyperintense	5.5	7.3	10.4	PR	-52.4	-46.3	8.9
16	Segment VI/VII	73	Hyperintense	5.7	6.6	11.6	PR	-65.8	-24.1	14.5[f]

[c]Lesion untreated
[d]Photopaenic lesion
[e]Patient died of unrelated illness
[f]Patient underwent liver transplant

SUV – standard uptake value
preRx – pretreatment
CR- complete response, PR – partial response, SD – stable disease, PD – progressive disease, NE – not evaluable

Table 2. Baseline Dynamic PET parameters (N=14)

Patient Number	**K_1 (mL/min/g)**	**k_2 (1/min)**	**k_3 (1/min)**	**k_4 (1/min)**	**v_B (mL/g)**	**K_i (mL/min/g)**
1	0.16	0.10	0.10	0.11	5.0E-101	0.08
2	0.17	0.076	0.074	0.07	0.015	0.09
3	0.31	0.40	0.24	0.04	0.019	0.11
4	0.21	0.28	0.13	0.06	0.034	0.07
5	0.34	0.17	0.097	0.04	0.03	0.13
6	0.43	0.28	0.086	0.01	0.058	0.10
8	0.282	0.28	0.13	0.02	0.04	0.09
9	0.29	0.53	0.32	0.04	0.05	0.11
11	0.41	0.51	0.17	0.02	0.07	0.10
13	0.11	0.16	0.04	0.001	0.10	0.02
14	0.46	0.42	0.13	0.03	2.9E-04	0.11
15	0.58	0.69	0.13	0.02	0.07	0.09
16	0.26	0.18	0.08	0.02	0.07	0.08
18	0.23	0.19	0.09	0.02	8.0E-06	0.07

SUPPLEMENTAL MATERIALS AND METHODS

Tissue Microarray

Access to retrospective tissue specimens was granted by the Imperial College Tissue Bank (Approval No. R16005). Following marking of diagnostic haematoxylin and eosin (H&E) slides, a MTA-1 Manual Tissue Microarrayer (Beecher Instruments, USA) was used to obtain 1 mm cores of matched cores of malignant tissue and surrounding cirrhotic parenchyma. The tissue cores were re-embedded in recipient microarray blocks. Both cancer and surrounding parenchyma were sampled in triplicate. Adequate sampling of the target lesions was confirmed on a freshly cut H&E section from the recipient TMA block before immunostaining.

Prospective Study Design and Participants

Eligible patients were aged 18-85 years with histological diagnosis HCC or a diagnosis of HCC based on American Association for the Study of Liver Diseases (AASLD) criteria, had intermediate stage disease suitable for TACE, disease evaluable by modified Response Evaluation Criteria in Solid Tumours (mRECIST) and at least 1 target lesion $\geq$20mm, an Eastern Cooperative Oncology group performance status (PS) of 2 or less, and a life expectancy of at least 6 months (*14*).

Patients had to have adequate bone marrow function (haemoglobin concentration >90 g/L, neutrophils >1500 cells per µL, platelets >100 000 cells per µL), kidney function (creatinine <1·5 times the normal upper limit; calculated creatinine clearance ≥50 mL/min), and liver function (aspartate aminotransferase or alanine aminotransferase ≤2·5 times the normal upper limit, alkaline phosphatase ≤2·5-times the normal upper limit, total bilirubin ≤1·5 times the normal upper limit).

Patients were recruited from Hammersmith Hospital, ICHNT. The study was approved by the London Bridge research ethics committee, ethics number 13/LO/1011. All the patients provided written informed consent. The study was conducted in compliance with the declaration of Helsinki.

A technical radiotracer production failure meant one patient out of 18 was unable to have baseline scanning and one patient withdrew consent following the first PET scan; therefore 16 patients were evaluable for treatment outcome

Imaging Protocol

18F-FLT was manufactured according to standard protocols. All patients were scanned on a Siemens Biograph 6 Truepoint at baseline and 6-8 weeks following TACE. An abdominal CT scan (300 mA, 120 kVp, 1.35 pitch, 0.8 s/rotation) for both attenuation correction and co-registration with PET images was performed, . 18F-FLT, mean (±SD) 208.2 ± 10.4 MBq, was injected as a bolus intravenously, and a dynamic, list mode emission scan in the 3D mode, lasting 66 min, was undertaken. Blood counting and metabolite analysis using the discrete blood samples during the scan at 5, 10, 15, 30 and 60 minutes were conducted(*15*).

Image Analysis

Raw PET data were corrected for scatter, attenuation and reconstructed with an iterative algorithm (8 iterations, 21 subsets). The data were binned into time frames as follows: 1 * 30 (background), 6* 10, 4* 20, 4* 30, 5* 120, 4* 180 and 4* 600 seconds. The KSF was applied to the dynamic PET data as previously reported(*16*). The attenuation corrected PET images (unfiltered and filtered) and CT data were fused and analysed on a dedicated workstation (Hermes diagnostics, Sweden) by a dual trained radiologist/ nuclear medicine physician (TDB). All SUV analyses were conducted using PET uptake parameters generated on Hermes. Tumour lesions were defined as target lesions by mRECIST on either CT or MRI(*17*).

For Kinetic Spatial Filter analysis, the 4D SUV images were smoothed in time (i.e. along the 4^{th} dimension) with a Gaussian smoothing kernel of unit standard-deviation. The temporal profile of each voxel in turn is compared against profiles for predefined classes. There are a number of possible filter rules. In this study we filtered out (i.e. excluded) voxels whose temporal profiles were “liver-like” by computing the Mahalanobis distance between the voxel profile and each tissue reference profile.

Quantitative Analysis

The Arterial Input Function.

For each patient, an additional ROI on the aorta was drawn for implementing an image derived arterial input function (idAIF) during kinetic modelling of data. Since metabolite data were available for 10 patients the idAIF was corrected for an average metabolite and plasma-over-blood ratio for each of these patients. The total 18F-FLT activity in each blood sample was averaged and used to fit the plasma-over-blood (POB) ratio to a mono-exponential curve to provide a continuous POB representation. A total plasma activity curve was obtained by multiplying the POB by the tissue-derived input function. Finally, the average pre- and post-treatment fraction of parent compound in each sample was fitted to obtain a continuous representation of the parent tracer concentration, which was then multiplied by the total plasma function. The result was a tissue-derived parent plasma input function for each scan that was subsequently used for compartmental modelling.

The Compartmental Model.

The average activity within the tumour ROI for each time-frame of the dynamic PET imaging sequence was used to generate regional tissue activity curves (TACs). The TACs, metabolite corrected idAIF and the whole blood activity curves were fitted to a two tissue compartmental model using the Levenberg-Marquart least-square minimization algorithm implemented in the PMOD kinetic modelling tool PKIN (PMOD version 3.703; PMOD group, Zurich, Switzerland). The two-tissue compartment model separates radiotracer in tissue into two exchanging compartments: C_1, which represents free and non-specifically bounded radiotracer in tissue, and C_2, which represents the specifically bounded radiotracer(*20*). The model is mathematically described by the following differential equations:

$$\frac{dC_1(t)}{dt} = K_1 C_p(t) - (k_2 + k_3) C_1(t) + k_4 C_2(t) \qquad 1)$$

$$\frac{dC_2(t)}{dt} = k_3 C_1 - k_4 C_2 \qquad 2)$$

The signal in a single voxel (C(t)) is then the combination of the signal in the two compartments:

$$C(t) = (1 - v_B)\big(C_1(t) + C_2(t)\big) + v_B C_B(t) \qquad 3)$$

K_1 represents the rate constant for transport of the tracer from blood into tissue (delivery), k_2 represents the rate constant of transfer from tissue back to blood, k_3 reflects the rate constant of phosphorylation of ^{18}F-FLT, k_4 describes the rate of dephosphorylation and v_B is the fraction of vascular activity in the tissue. C_p and C_B are the

tracer activity concentration in the plasma and in the blood, respectively. The residuals were weighted by the inverse of the variance that takes into account the measured uptake, the radioactive decay and the duration of the acquisition:

$$\sigma^2 = \alpha^2 \frac{C_{PET}(t_i)}{\Delta t_i e^{-\lambda t_i}} \qquad 4)$$

with a scale factor α^2, the decay-corrected uptake $C_{PET}(t_i)$ at frame mid-time t_i, the frame duration Δt_i, and the decay constant λ, which is obtained from the half-life $T_{1/2}$ of the isotope (*21*). The FLT flux, K_i, was derived using the compartmental model parameters(*21*):

$$K_i = \frac{K_1 \cdot k_3}{k_2 + k_3} \qquad 5)$$

The two-tissue compartmental model was tested with and without the k_4 parameter to address the noisy nature of the last frames of the dynamic PET scan. The comparison between the two models was tested with the Akaike Information Criteria (AIC) and, with the k_4 included in the model, lower AIC values were obtained ($p < 0.05$).

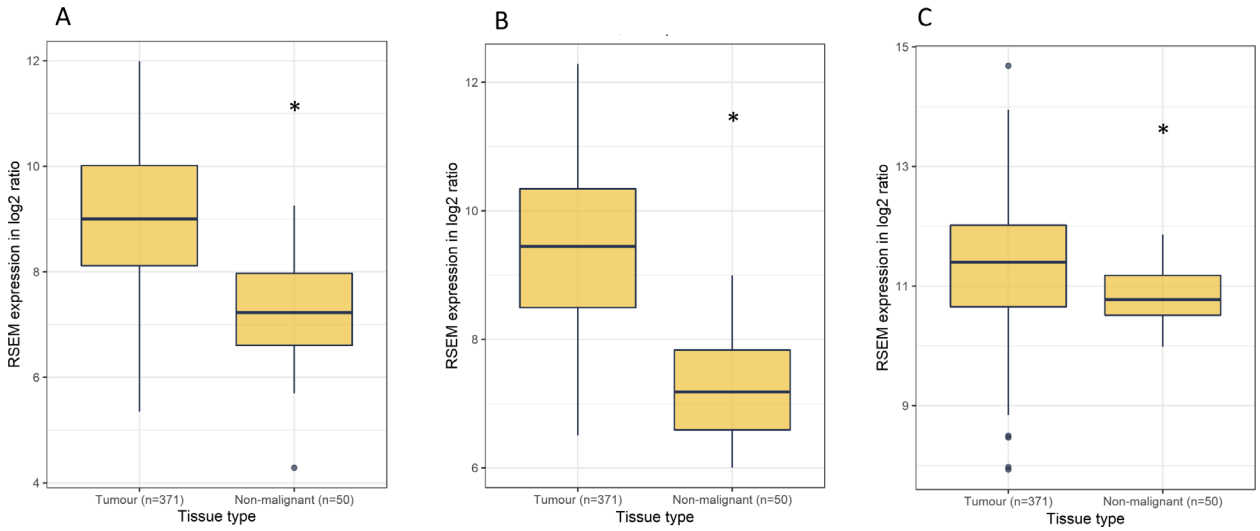

Supplemental Figure 1. Relative RNA expression of *TYMS* (A), *TK-1* (B) and *SLC29A1* (C) in HCC (n=371) and non-malignant tissue (n=50), Cancer Genome Atlas, * p<0.05

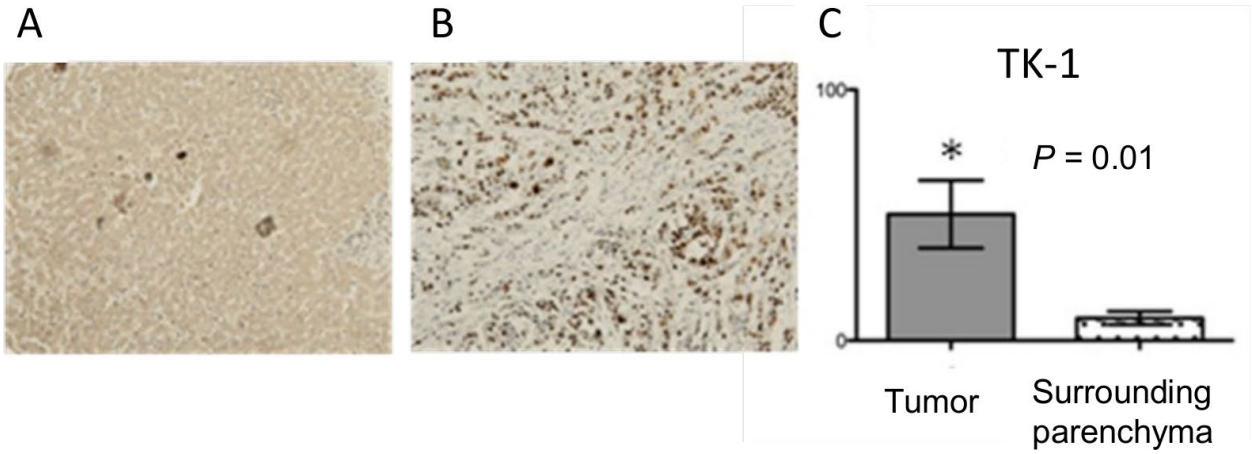

Supplemental Figure 2. Represented sections illustrating TK-1 expression by immunohistochemistry (1:100, AbCam, Cambridge) on **(A)** liver parenchyma and **(B)** HCC. A significant increase in the expression of TK-1 (histoscore) was observed in HCC compared to surrounding liver parenchyma **(C**) * p=0.01

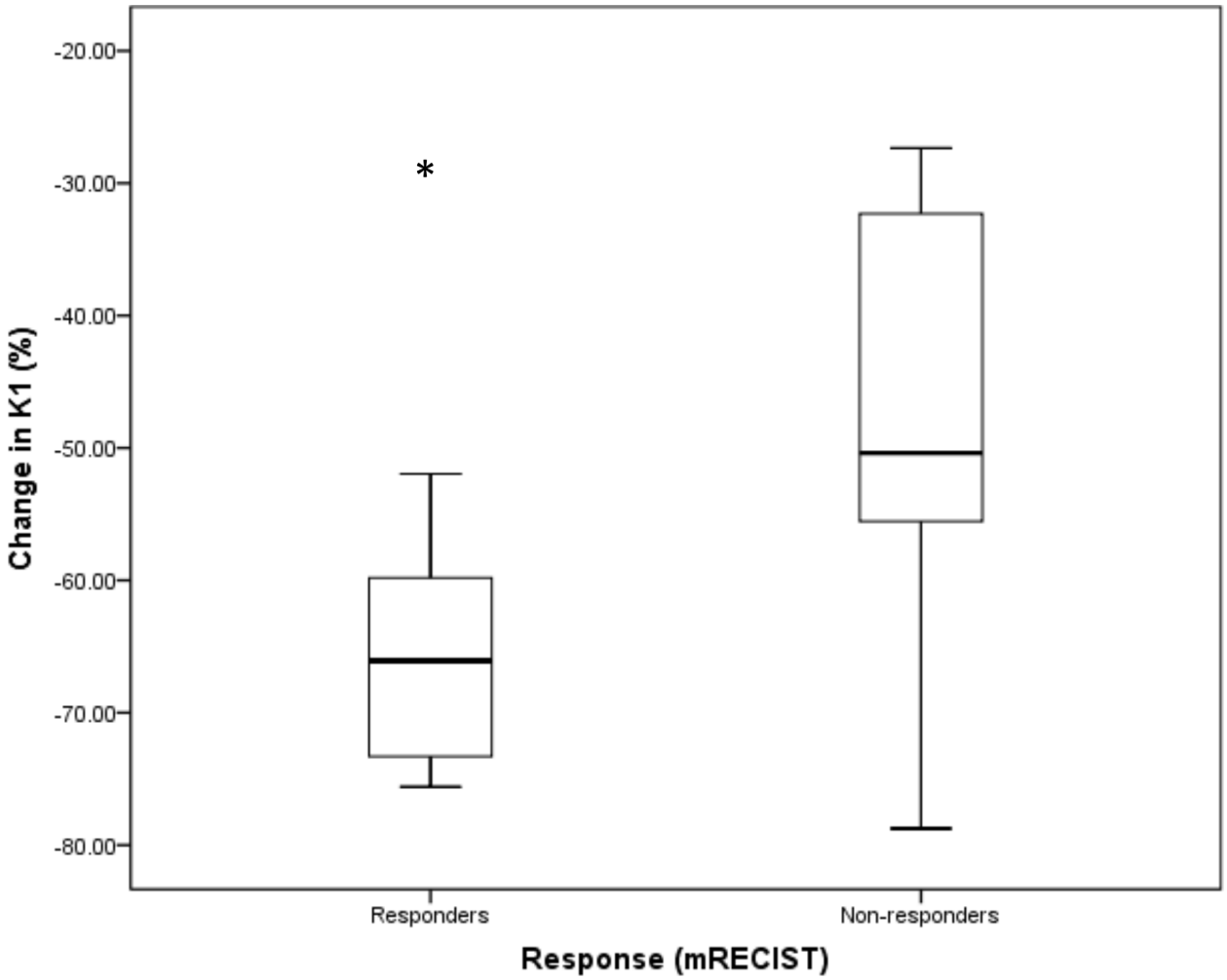

Supplemental Figure 3A: Percentage change in K_1 in responders and non-responders, * $p<0.05$,

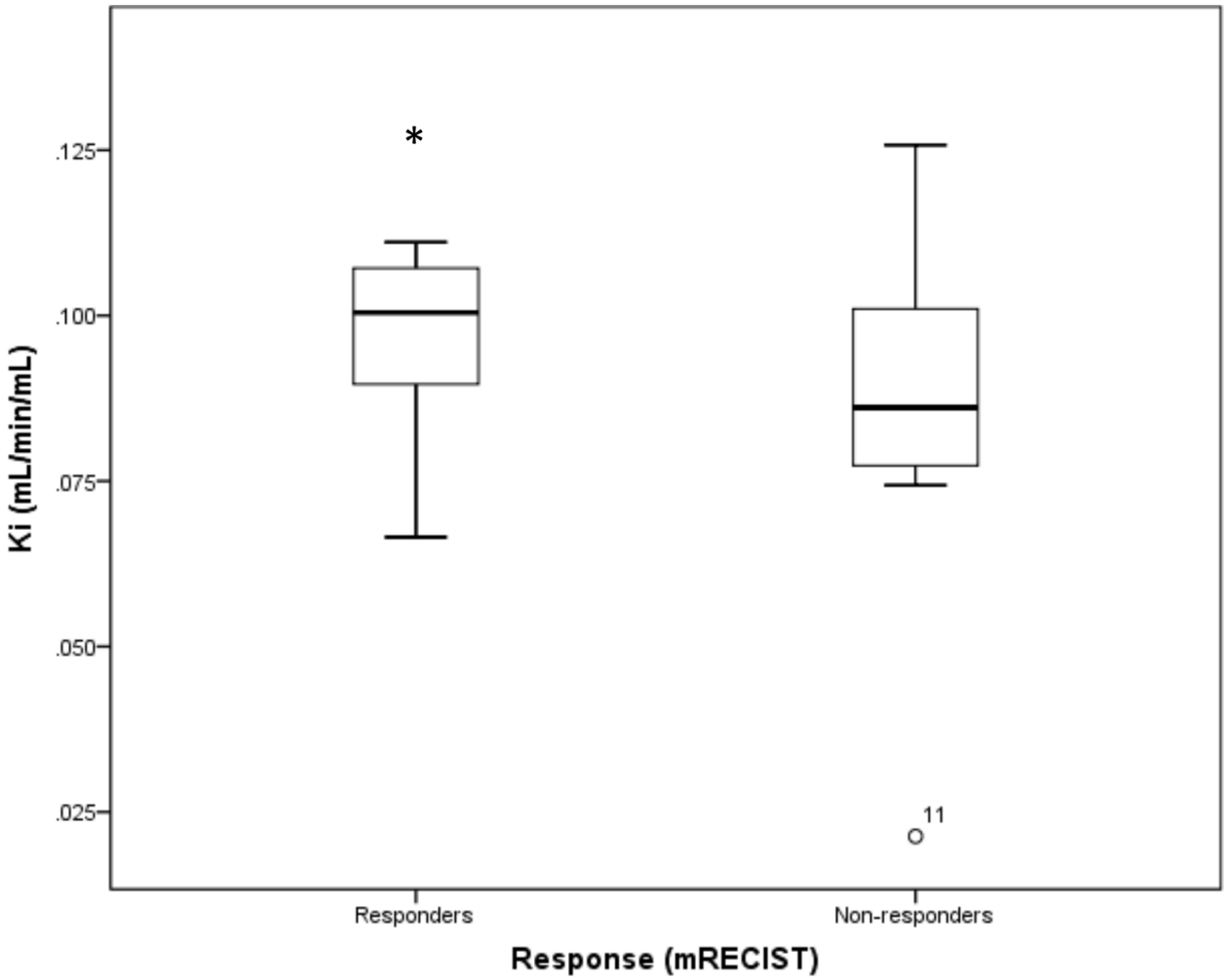

Supplemental Figure 3B: Baseline K_i in responders and non-responders, * $p<0.05$

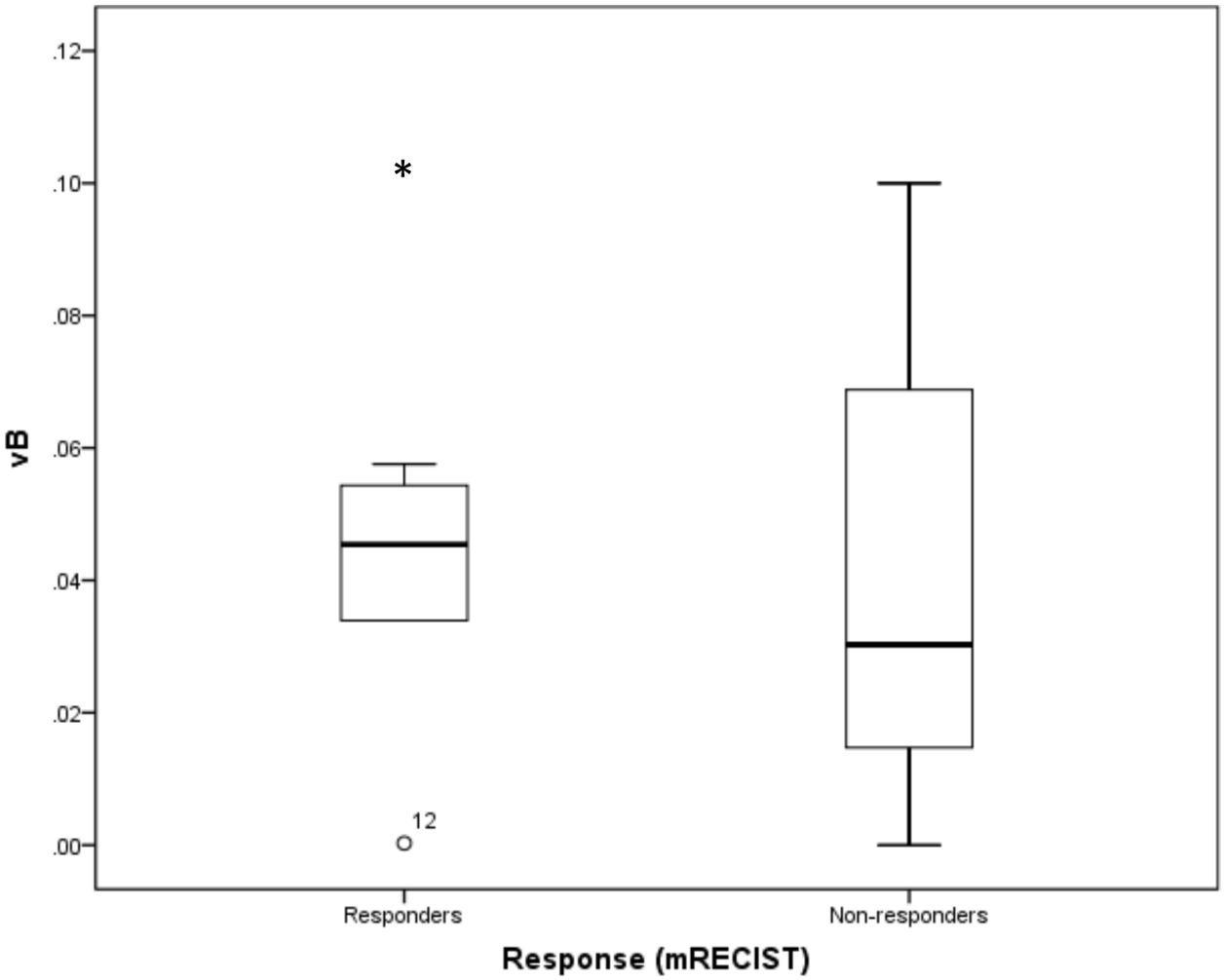

Supplemental Figure 3C: Baseline v_B in responders and non-responders, * $p<0.05$